Journal of Power Sources 399 (2018) 49–58

Contents lists available at ScienceDirect

Journal of Power Sources

journal homepage: www.elsevier.com/locate/jpowsour

Multi-walled carbon nanotube-wrapped SiP_2 as a superior anode material for lithium-ion and sodium-ion batteries

Ching-Yu Wang, Yuan-Hsing Yi, Wei-Chung Chang, Tzu-Lun Kao, Hsing-Yu Tuan*

Department of Chemical Engineering, National Tsing Hua University, Hsinchu, 300, Taiwan

HIGHLIGHTS

- MWCNT-wrapped SiP_2 anodes for LIBs and SIBs is fabricated.
- MWCNT-wrapped SiP_2 shows a capacity of 1622 mA h g^{-1} at 0.5 A g^{-1} in LIBs.
- MWCNT-wrapped SiP_2 shows a capacity of 925 mA h g^{-1} at 0.2 A g^{-1} in SIBs.
- Coin-type and pouch-type full cells were assembled using SiP_2 anodes.

GRAPHICAL ABSTRACT

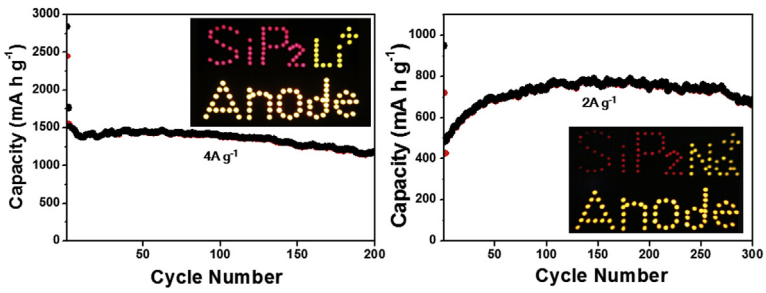

ARTICLE INFO

Keywords:
Silicon diphosphide
Carbon nanotube
Lithium ion battery
Sodium ion battery
Anode material

ABSTRACT

SiP_2 has a high specific theoretical capacity of 2902 mA h g^{-1} as an anode material for lithium-ion batteries and 1788 mA h g^{-1} for sodium-ion batteries, respectively, but demonstrates very poor cycling stability in the entire voltage range (0–2 V). Here, we report high performance SiP_2 anodes for lithium-ion batteries and sodium-ion batteries with good cycling stability by wrapping SiP_2 with multi-walled carbon nanotube (MWCNT) on the surface of SiP_2 via a ball milling prociess. MWCNT provides a robust network to connect fragment SiP_2 with surrounding electrical conductor and serves as an effective conductive agent. MWCNT-wrapped SiP_2 shows a reversible capacity of 1622 mA h g^{-1} after 100 cycles at 0.5 A g^{-1} in lithium-ion batteries and 925 mA h g^{-1} after 200 cycles at 0.2 A g^{-1} in sodium-ion batteries. In addition, rate capability is significantly enhanced. Furthermore, both coin-type and pouch-type full cells are assembled using SiP_2 anodes which are coupled respectively with a cathode of $LiFePO_4$ for lithium-ion batteries and a cathode of $Na_{2/3}Ni_{1/3}Mn_{2/3}O_2$ for sodium-ion batteries, and supplied as a reliable energy source for electronic uses to evaluate practical applications.

1. Introduction

Lithium ion batteries (LIBs) and sodium ion batteries (SIBs) with higher energy and power densities are needed for batteries applicable for advanced technologies [1,2], including hybrid electric vehicles (HEV), electric vehicles (EV), intelligent grid and renewable energy technologies. In the past 25 years, intercalation-type anode plays a critical role in commercial batteries, however, graphite's low theoretical specific capacities of graphite in LIBs (372 mA h g^{-1}) and SIBs (35 mA h g^{-1}) can't comply with increasing demand of energy storage, therefore, high specific capacity elements are proposed as graphite alternatives, such as silicon (Si), phosphorus (P), and germanium, etc. [3–9].

Silicon (Si) is a promising graphite alternative for LIBs due to its high theoretical capacity of 3578 mA h g^{-1}. Nonetheless, Si occurred massive volume change of about 300% during repeated lithiation-

* Corresponding author.
E-mail address: hytuan@che.nthu.edu.tw (H.-Y. Tuan).

https://doi.org/10.1016/j.jpowsour.2018.07.003
Received 13 April 2018; Received in revised form 14 June 2018; Accepted 1 July 2018

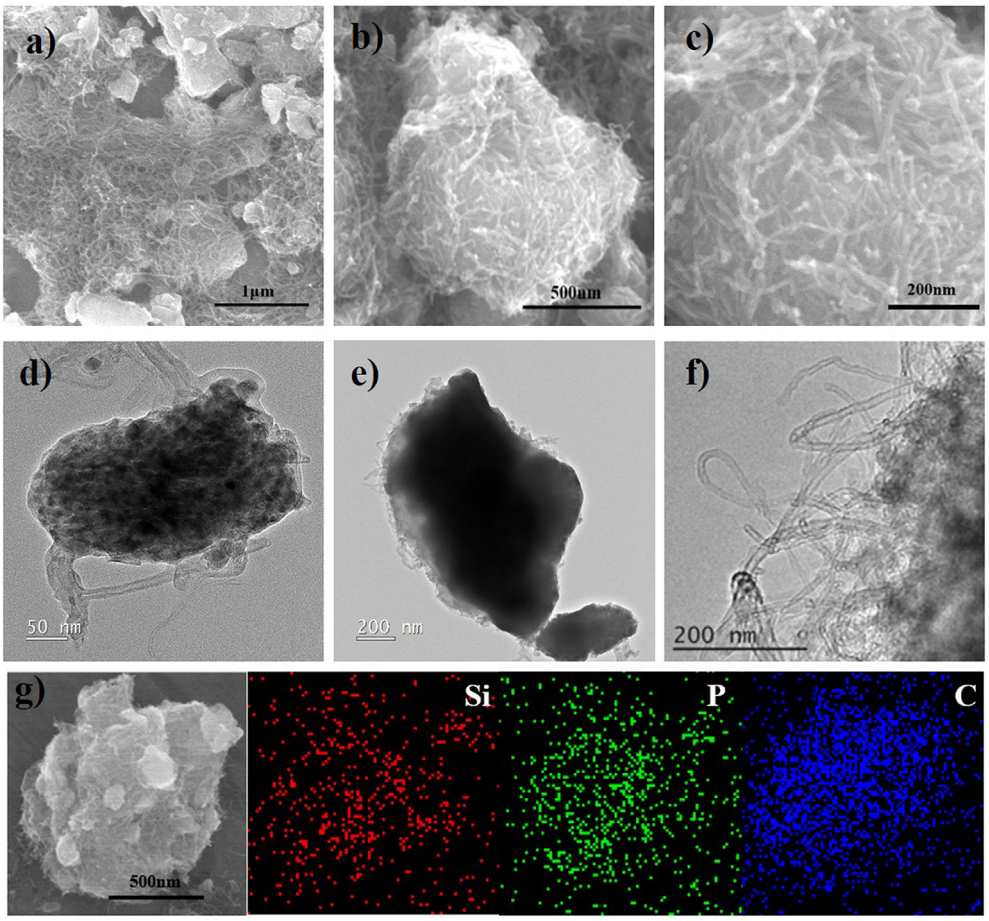

Fig. 1. (A-c) SEM images of MWCNT-wrapped SiP_2 (d–f) TEM images of MWCNT-wrapped SiP_2 (g) SEM image and corresponding EDS mapping images of MWCNT-wrapped SiP_2.

delithiaton processes which results in electrode pulverization. One effective strategy to address this problem is to use active/inactive composite materials, i.e., Si-X (X = Li active/inactive element) compounds, as an active material. For example, Si-X compounds, such as Co [10], Ni [11], Fe [12], Cu [13], can improve electrical conductivity and capacity retention since inactive metal can mitigate large volume expansion. On the contrary, Si-X compound employing Li-active metals, such as O [14], Ca [15], Mg [16], Sn [17], enhance electrochemical performance of anodes owing to enhanced electrical conductivity and matrix of inactive component. On the other hand, phosphorus (P) has the second highest theoretical capacity of 2596 mA h g^{-1} in LIBs, making it another attractive graphite alternative. Besides, P has the highest theoretical capacity (2596 mA h g^{-1}) in SiBs, whereas Si has low level activity with sodium ions. However, P also meets capacity degradation resulted from large volume expansion during lithiation-delithiation or sodiation-desodition processes and behaves like an insulator [18,19]. Several metal phosphides (MP, M = transition metal), such as FeP [20], FeP_2 [21] CoP [22], Cu_3P [23], and CuP_2 [24], have been suggested, but it prefers to prepare P-based compounds with other high specific capacity elements [25–27].

SiP_2 has a theoretical capacity of 2902 mA h g^{-1} in LIBs, which is superior to that of P. SiP_2 can react with sodium ions to form Na_3P that possess a theoretical capacity of 1788 mA h g^{-1} in SIBs [25,26]. Moreover, SiP_2 has a unique 3D crystalline framework structure to effectively improve electrochemical performance of Si and P within different voltage range in LIBs. In the electrochemical analysis with voltage range between 0.25 V and 2 V, and voltage between 0.55 V and 2 V, SiP_2 shows an outstanding retention of 98.8% and 99.9% after 100 cycles respectively; however, the narrow voltage range substantially limits capacities of SiP_2, which only has a capacity of 1100 mA h g^{-1} operated from 0.25 V to 2 V and 500 mA h g^{-1} from 0.55 V to 2 V, respectively). In the entire voltage range (0–2 V), SiP_2 shows unstable cycling performance after 100 cycles with retention less than 50%.

We show that SiP_2 wrapped with multi-walled carbon nanotubes (MWCNT) has significantly improved cycle ability and rate capability for both LIBs and SIBs in the entire voltage range (0–2 V). MWCNT–wrapped SiP_2 was prepared via a ball milling process. The electric measurement of MWCNT-wrapped SiP_2 pellets exhibits conductivity five times higher than that of pristine SiP_2. MWCNT not only improves conductivity, but also provides a robust network to SiP_2 anodes, resulting in superior cycling performance of 1622 mA h g^{-1} after 100 cycles at a current density of 0.5 A g^{-1} and 1522 mA h g^{-1} at 4 A g^{-1} in LIBs, and 925 mA h g^{-1} after 200 cycles at 0.2 A g^{-1} and 491 mA h g^{-1} at 2 A g^{-1} in SIBs. The anode performance of MWCNT-wrapped SiP_2 anodes ranks as the best anode performances on a basis of SiP_2-related anode to date. Finally, the full cells assembled with MWCNT-wrapped SiP_2 anode were coupled respectively with a cathode of $LiFePO_4$ in LIBs and a cathode of $Na_{2/3}Ni_{1/3}Mn_{2/3}O_2$ in SIBs that were used to verify the feasibility of MWCNT-wrapped SiP_2 as anodes on practical battery designs.

2. Result and discussion

Alloy-type electrodes/carbon composite were often prepared to address the issue of poor electrochemical performance. Active materials milled with a variety of carbon sources such as graphene [28,29], carbon black [30,31], graphite [32,33], and carbon nanotubes [34,35] can improve electrical conductivity and alleviate volume expansion

since active materials are embedded into carbon matrix effectively. We choose carbon nanotube as composite carbon source since it provides beneficial electrical conductivity, strong architectures, and mechanical resilience for active materials. Fig. S1 shows the illustration of the preparation of MWCNT-wrapped SiP_2. SiP_2 was firstly prepared by ball milling of silicon and phosphorus, and the resulting SiP_2 was then ball milled again with the presence of MWCNT. Compared with black phosphorus, which react with oxygen to form P_xO_y [36,37], SiP_2 is chemically stable in the atmosphere. In the crystalline structure of SiP_2, lone pair occupied by silicon may prevent the reaction between phosphorus and oxygen. Fig. S2 shows the XRD pattern of the MWCNT-wrapped SiP_2 phase, which precisely corresponded to cubic SiP_2 (JCPDS-751288) and MWCNT (JCPDS-752078) and there was no new phases in the XRD pattern. In Fig. 1a and c, the SEM images of the products show that SiP_2 were densely entangled by MWCNT. In Fig. 1d and f, the TEM images also reveal that MWCNT was coiled on the surface of SiP_2. In Fig. 1g, energy-dispersive spectroscope (EDS) elemental mappings of the MWCNT-wrapped SiP_2 clearly performed the homogeneous distribution of the Si, P and C elements (red, green and blue represent the elements of Si, P and C, respectively). To confirm the crystallographic properties of the SiP_2, high resolution TEM (HRTEM) investigation was performed. The HRTEM images of SiP_2 in Figs. S3a and S3b showed clear crystalline nature, and the corresponding fast Fourier transform (FFT) (inset of Fig. S3b) patterns show the same result. The measured *d*-spacing of 0.188 nm and 0.203 nm between the adjacent lattice planes corresponds to the {221} and {20$\bar{2}$} plane respectively. The current-voltage (I-V) characteristics of MWCNT-wrapped SiP_2, Si and Ge pellets with an area of 0.25 cm^2 were conducted to measure electrical conductivity as shown in Fig. 2a and b. SiP_2 has electrical conductivity with several orders of magnitude higher than Si and P, although the conductivities of Si and P were both poor. This phenomenon may be resulted from P doping effect in SiP_2 [38,39]. MWCNT apparently enhances the conductivity of SiP_2 about five times and the advance of electrical conductivity could effectively promote electrochemical performance such as rate capability and cycling performance.

The electrochemical performance of the MWCNT-wrapped SiP_2 LIB anode was tested by coin-typed half-cell (CR2032) using a lithium metal foil as counter electrode within the range of 0.01 V–2.0 V. Fig. 3a shows the voltage profile of MWCNT-wrapped SiP_2. During the discharge process, the voltage sharply decreased from open circuit voltage to 0.7 V where a plateau observed. The other plateau appears at about 0.2 V, then the voltage further decreasing slowly to 0.01 V. These plateaus indicate phase transformation due to lithium-ion insertion. In a charge process, two plateaus were observed at 0.6 V and 1.1 V to illustrate the removal of the lithium-ion from active materials. Fig. 3b shows the differential capacity profiles of the 1st, 10th, and 20th cycle. The peaks indicate insertion reaction of Li ions, and the presence of sharp peaks suggest that different react phases. Fig. 3c shows the cycling performance of MWCNT-wrapped SiP_2, pristine SiP_2, and MWCNT at a current density at 0.5 A g^{-1}. The first discharge and charge specific capacity of MWCNT-wrapped SiP_2 were 2642 and 2131 mA h g^{-1} respectively, corresponding to a Coulombic efficiency nearly 80%. The capacity contributed by MWCNT in MWCNT-wrapped SiP_2 composite is negligible by their significantly lower capacities (~170 mA h g^{-1}) as a LIB anode. The irreversible capacity was mainly caused by forming a SEI layer on the electrode during the first discharge and charge processes. After the first cycle, subsequent cycles showed the highly reversible capacity without apparent fading compared with SiP_2 after 100 cycles. The 100^{th} cycle exhibited a specific capacity of charge 1622 mA h g^{-1}, which maintained the nearly 93% charge capacity of the 5 t h cycle. The plateaus is same between 1st cycle and 100^{th} cycle. In addition to reaction with lithium, there are no other side reaction shows the electrochemical stability is stable. On the other hand, the first discharge and charge specific capacity of SiP_2 were 2281 and 1980 mA h g^{-1} respectively; however, in the sequential cycles, SiP_2 shows apparent decay. After 100 cycles, MWCNT-wrapped SiP_2 and SiP_2 exhibit 93% and 22.3% retention. Electrochemical performances of SiP_2 studies reported in LIBs were summarized in Table 1. The anode performance of MWCNT-wrapped SiP2 anodes ranks as the best anode performance to date. The interfacial electrochemical behavior difference of MWCNT-wrapped SiP_2 electrode after cycling was investigated by means of electrochemical impedance spectroscopy (EIS), which was carried out from 10 kHz to 10 mHz. In the Nyquist plots (Fig. 3d), the semicircle part represents the charge transfer resistance, resulting from the occurrence of polarization of electrode as leaving open-circuit equilibrium state. It was obvious that the corresponding semicircle of the electrode that experienced 50 cycles was extremely smaller than that of the as-prepared electrode, indicating a decrease in charge transfer resistance from 150 Ω to 20 Ω, suggesting improved electron transfer and lithium ion diffusion.

The comparison between rate-capability of MWCNT-wrapped SiP_2 and SiP_2 were evaluated by increasing the discharge/charge rate from 0.2 A g^{-1} to 30 A g^{-1}, as shown in Fig. 4a, and its corresponding voltage profiles are shown in Fig. 4b. MWCNT-wrapped SiP_2 showed an outstanding rate performance between 0.2 A g^{-1} and 30 A g^{-1}, displaying specific charge capacities of 2053, 1753, 1636, 1547, 1473, 1250, 1071, 791, and 391 mA h g^{-1} at current densities of 0.2 A g^{-1}, 1 A g^{-1}, 2 A g^{-1}, 4 A g^{-1}, 6 A g^{-1}, 10 A g^{-1}, 14 A g^{-1}, 20 A g^{-1} and 30 A g^{-1}, respectively. Compared with of SiP_2 without MWCNT, MWCNT-wrapped SiP_2 showed significant improvement in rate-capability. As shown in Fig. 4c, MWCNT-wrapped SiP_2 showed good cycling life of 200 cycles at high current density of 4 A g^{-1}.

The photograph of pristine SiP_2 electrode shows severe

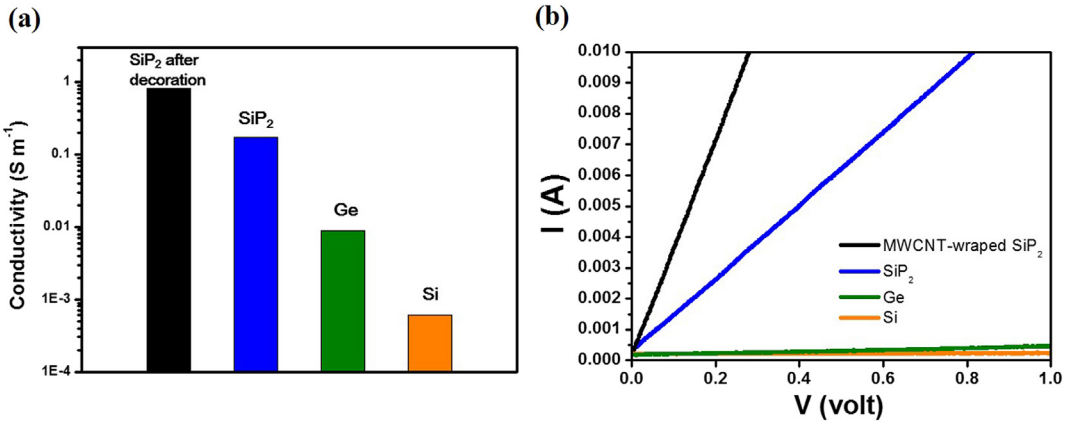

Fig. 2. Electric characteristics of MWCNT-wrapped SiP_2, SiP_2, Ge, and Si (a) conductivities of MWCNT-wrapped SiP_2, SiP_2, Ge, and Si (b) I-V curves of MWCNT-wrapped SiP_2, SiP_2, Ge, and Si.

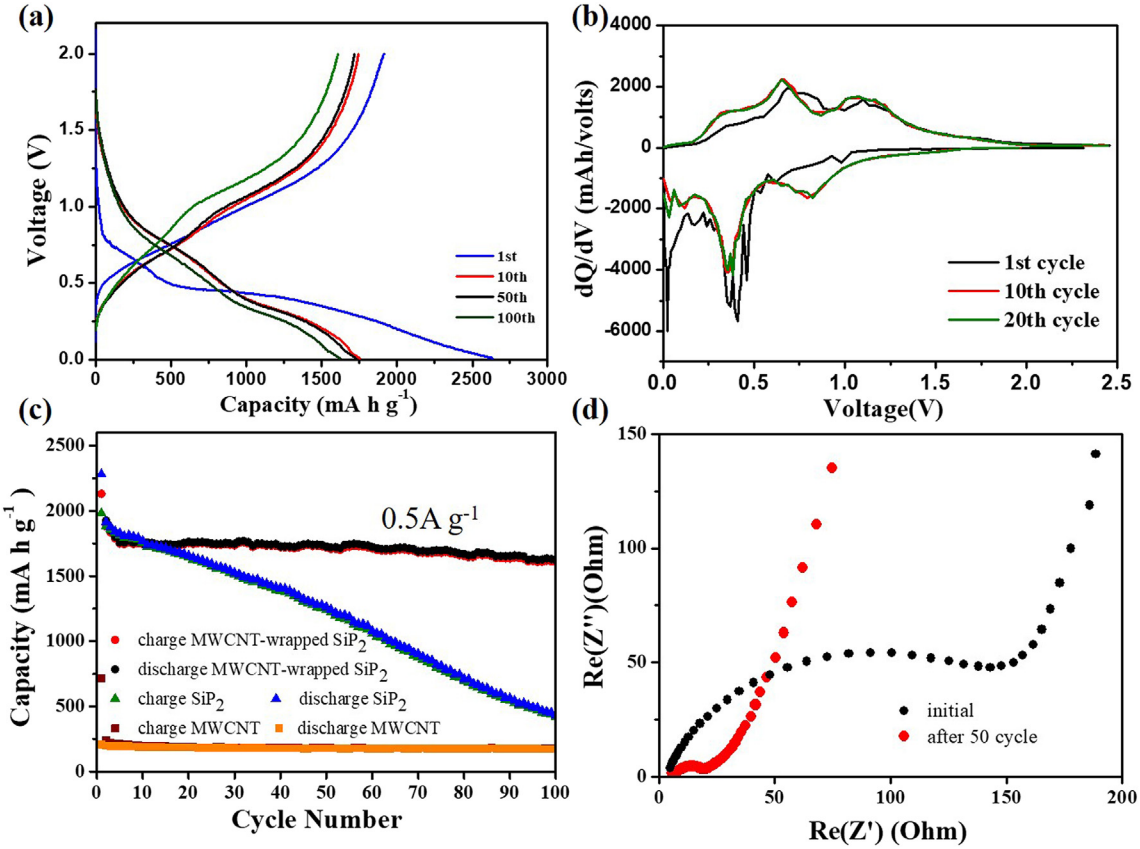

Fig. 3. Electrochemical performances of MWCNT-wrapped SiP_2 in LIBs (a) voltage profiles of MWCNT-wrapped SiP_2 at 0.2 A g^{-1} between 0.01 V and 2.5 V (b) differential capacity profile of the first, 10th, and 20th cycles of MWCNT-wrapped SiP_2 (c) charge/discharge cycle performance of MWCNT-wrapped SiP_2, SiP_2, and MWCNT at 0.5 A g^{-1} for 100 cycles (d) electrochemical impedance spectroscopy of fresh MWCNT-wrapped SiP_2 electrode and that of the electrode, which experienced a 50 cycling test.

Table 1
Comparison of the electrochemical performance of different SiP_2 electrodes for LIBs.

Active material	Capacity (5th cycle)	Capacity (100th cycle)	retention	Reference
MWCNT-wrapped SiP2	1760 mA h g^{-1}	1622 mA h g^{-1}	93%	This work
SiP_2	1822 mA h g^{-1}	435 mA h g^{-1}	24%	This work
SiP_2	~1350 mA h g^{-1}	~500 mA h g^{-1} (10 cycle)	37%	[25]
SiP_2/C	~1700 mA h g^{-1}	~700 mA h g^{-1}	41%	[25]
SiP_2/C	~2000 mA h g^{-1}	~1000 mA h g^{-1} (30 cycle)	50%	[26]

delamination of active materials from copper foil surface after 100 cycle charge/discharge at a current density of 4 A g^{-1} (Fig. S4a). Before lithiation, SiP_2 particles show uniformly dispersion with binder and conductive agent (Fig. S4b), but obviously disintegrated and collapsed after cycling (Fig. S4c). On the other hand, the surface of MWCNT-wrapped SiP_2 electrode still remained intact after cycles (Fig. S4e). MWCNT can secure the SiP_2 particle to prevent particle cracking and fracture (Fig. S4d). SEM images with higher magnification further prove that MWCNT can capture fragment of SiP_2 during cycling (Fig. S4h).

The full cells consisting of MWCNT-wrapped SiP_2 anode and commercial $LiFePO_4$ cathode verify the practical application of MWCNT-wrapped SiP_2 anode. In Fig. S5a, the charge simulation of full cells shows an appropriate voltage range of MWCNT-wrapped SiP_2 full cells obtained by subtracting the charge curve of $LiFePO_4$ from the discharge curve of the MWCNT-wrapped SiP_2 in their respective half-cells. The MWCNT-wrapped SiP_2-$LiFePO_4$ charge curve full cell should be located between 2 V and 3.5 V, and the plateau of discharge curve was about 2.8 V and 3.2 V. In Fig. S5b, the MWCNT-wrapped SiP_2-$LiFePO_4$ full cell discharge curve was plotted in the same way, ranging from 3.2 V to 2 V. The plateau of discharge curve was about 2.8 V and 2.4 V. Therefore, the full cell cutoff voltage of discharge and charge should be set between 2 V and 4 V respectively. Few capacities could be obtained below 2 V and above 4 V. Moreover, the lower voltage led to limited application and higher voltage probably resulted in side reaction respectively.

As shown in Fig. 5a, cycling performance of the coin-typed full cells at current density about 0.4 A g^{-1} and a areal capacity about 1.6 mA h/cm^2, displayed a specific charging density of 2151 mA h g^{-1} and good retention about 95.5% after 50 cycles (respect to 2nd cycle), indicating high potential for use in practical application. The voltage profiles at 1st, 10th, 20th, and 40th cycle (Fig. 5b) exhibit several potential plateaus during the discharge and charge cycles. In the charge process potential plateaus at 2.5–3.5 V and in the discharge process voltage curve at 3.0–2.0 V. These results both correspond approximately with the simulation. As shown in Fig. 5c, coin-typed full-cell at high current density (4 A g^{-1}) exhibits high retention (94% respective to 2nd cycle) after 150 cycles, indicating high utilization of MWCNT-wrapped SiP_2. To further facilitate MWCNT-wrapped SiP_2 applications, high capacity (35 mA h) pouch type full cell (Fig. 5d and e) was fabricated, showing satisfactory performance after 50 cycle with 85% retention and successfully applied to light up more than 100 LEDs with red, yellow, and orange color (Fig. 5f).

We also evaluate the electrochemical performance of the MWCNT-wrapped SiP_2 composites as SIB anodes, which were assembled in coin-

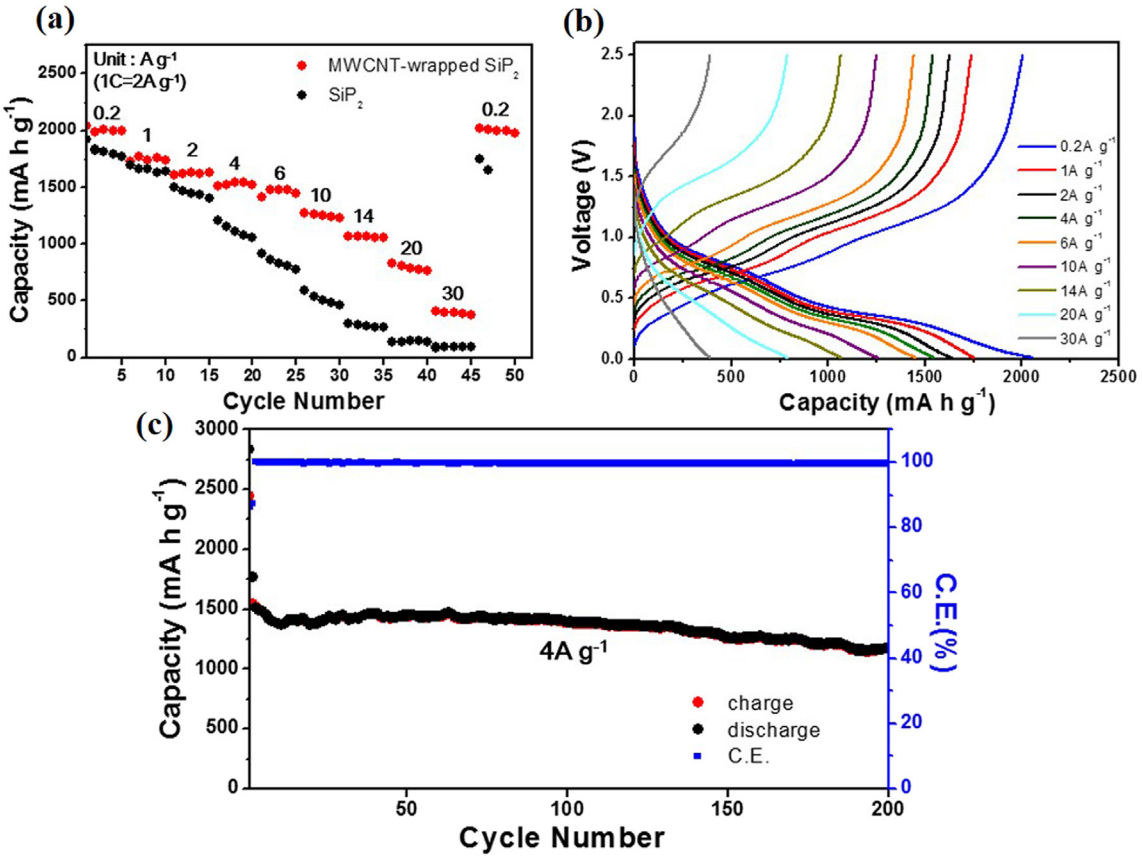

Fig. 4. (A) The rate performances of MWCNT-wrapped SiP_2 and SiP_2 electrode at various current density from 0.2 A g^{-1} to 40 A g^{-1} in LIBs (b) the corresponding voltage profiles of (a) with various current density from 0.2 A g^{-1} to 40 A g^{-1} (c) the cycling performance of MWCNT-wrapped SiP_2 at a current density of 4 A g^{-1} over 200 cycles in LIBs.

typed half-cells (CR2032) with sodium metal foil as counter electrode within the range of 0.01 V–2.5 V. Fig. 6a shows the voltage profile of MWCNT-wrapped SiP_2. During the discharge process, the voltage rapid declined to a plateau at 0.5 V which illustrated the transformation of active material due to the insertion of sodium ions. The voltage further decreased slowly to 0.01 V to form the final phase. In the charge process, a plateau was observed at 0.7 V–1.1 V, which represent the evacuation of sodium ions. Fig. 6b exhibits the differential capacity profiles of the 1st, 10th, 50th, and 100th cycle. The different peaks indicate different insertion reactions of Na ions, and each sharp peak suggests different reaction phase. Fig. 6c shows cycling performance of the MWCNT-wrapped SiP_2, SiP_2 and MWCNT with the current density at 0.2 A g^{-1}. The first discharge and charge specific capacity of MWCNT-wrapped SiP_2 were 1009 and 737 mA h g^{-1} respectively, which indicates a Coulombic efficiency of 73%. The capacity contributed by MWCNT in MWCNT-wrapped SiP_2 composite is negligible by their significantly lower capacities (~50 mA h g^{-1}) as an SIB anode. The irreversible capacity loss in the first cycle probably resulted from the consumption of sodium of solid electrolyte interface (SEI) layer. Surprisingly, the specific capacity displayed slightly rise in each subsequent cycle. This phenomenon could be attributed to strong chemical bonding between Si and P. In LIBs, both Si and P reacted with lithium ions. However, in SIBs, only P reacted with sodium ions, making chemical bonding between Si and P more too strong to be broken than that in LIBs. Tough chemical bonds limit phosphorus reactivity, leading to specific capacity less than the theoretical capacity, i.e., 1788 mA h g^{-1}, with silicon being participated in SIBs. Furthermore, this phenomenon also provides space of unreactive material to alleviate mechanical stress during charge/discharge process. After 200 cycles, the specific capacity of charge was 920 mA h g^{-1}, approaching to a nearly 132% relative to charge capacity of the 5th cycle, and is higher than the reported value (Table 2). We can see the same plateaus between 1st cycle and 200th cycle, indicating that there are no other side reactions and show good electrochemical stability. On the other hand, the first discharge and charge specific capacity of SiP_2 were 580 and 347 mA h g^{-1} respectively. The specific capacity of SiP_2 without MWCNT shows noticeable deterioration after 100 cycles. Apparently, MWCNT-wrapped SiP_2 showed better electrochemical performance than SiP_2 without MWCNT; besides, it also had higher specific capacity than that of pristine SiP_2. This increment may be resulted from higher chemical reactivity and electrical conductivity provided by MWCNT. Importantly, electrochemical performance of MWCNT-wrapped SiP_2 shows significantly improved performance compared to the previous studies of SiP_2 sodium ion anodes, The rate-capability improvement of SiP_2 wrapped by MWCNT in SIBs was also confirmed by changing the discharge/charge rate from 0.2 A g^{-1} to 15 A g^{-1} as shown in Fig. 7a. Compared to SiP_2, MWCNT-wrapped SiP_2 showed extreme rate performance between 0.2 A g^{-1} and 15 A g^{-1}, displaying the specific charge capacities of 608, 634, 555, 491, 414, 314, 230, 157, 47 mA h g^{-1} at the current density of 0.2 A g^{-1}, 0.5 A g^{-1}, 1 A g^{-1}, 2 A g^{-1}, 3 A g^{-1}, 5 A g^{-1}, 7 A g^{-1}, 10 A g^{-1}, and 15 A g^{-1}, respectively. As shown in Fig. 6c, MWCNT-wrapped SiP_2 exhibited excellent cycling life of 200 cycles at current density of 2 A g^{-1}. Initially, the current density 0.1 A g^{-1} for the first cycle was adapted to form an elegant SEI layer on active material surface. At the 300th cycle, the retention of MWCNT-wrapped SiP_2 composite specific capacity approached 143% relative to the 2nd cycle and 93.7% relative to the 100th cycle. These results apparently indicated that cycling performance and rate-capability of active materials were effectively promoted by MWCNT.

Sodium ion full cells were assembled with MWCNT-wrapped SiP_2 as

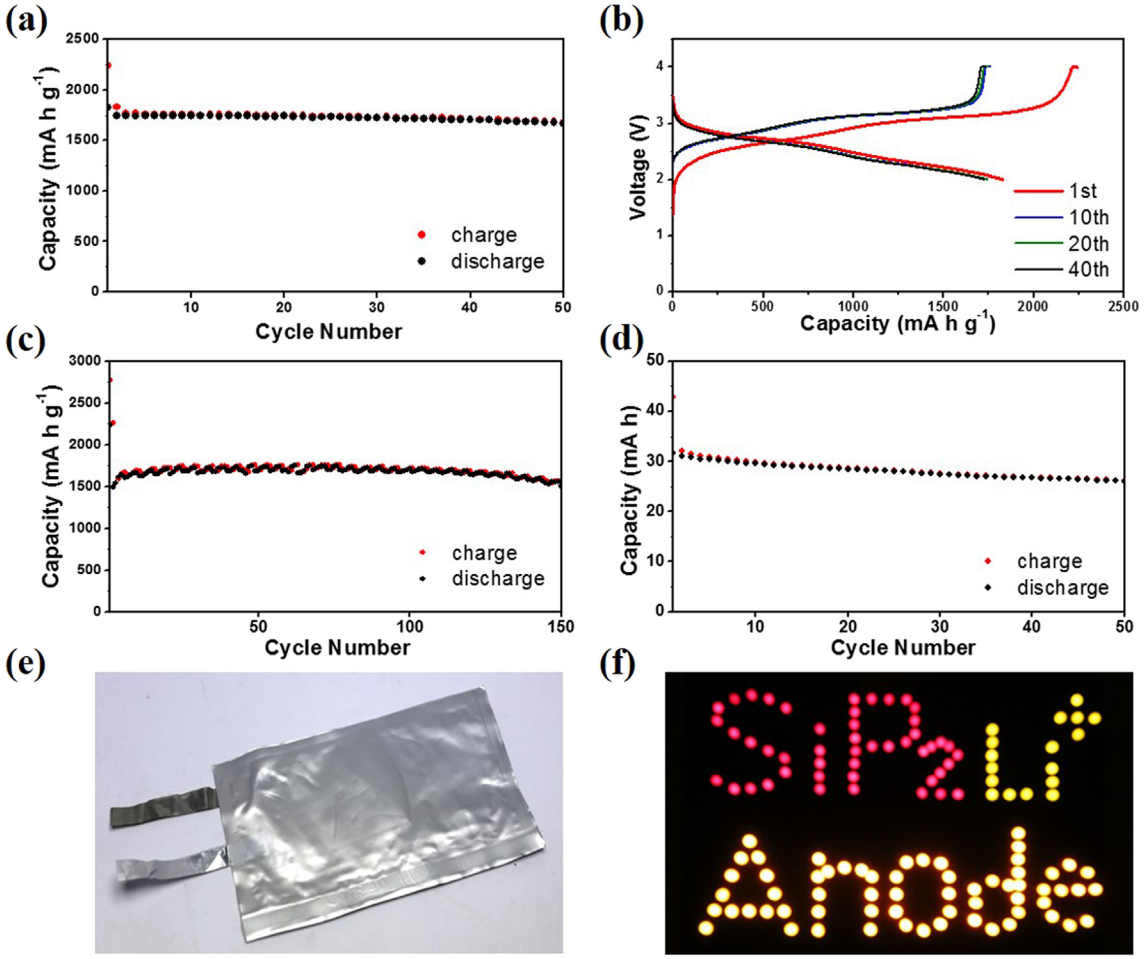

Fig. 5. Electrochemical characteristics of MWCNT-wrapped SiP_2/$LiFePO_4$ full cells. (a) cycling performance of coin cell at a current density of 0.4 A g^{-1} based on anode between 2.0 V and 4.0 V (b) the voltage profiles of coin cell at a current density of 0.4 A g^{-1} based on anode between 2.0 V and 4.0 V (c) cycling performance of coin cell at a current density of 2 A g^{-1} (d) cycling performance of pouch type cell with capacity (35 mA h) at a current density of 0.2 A g^{-1} (e) the photograph of a 35 mA h pouch type battery (f) the demonstration of pouch-type battery lighting up over 100 LEDs with different colors. (For interpretation of the references to color in this figure legend, the reader is referred to the Web version of this article.)

anodes and $Na_{2/3}Ni_{1/3}Mn_{2/3}O_2$ (NNMO) as cathodes. The synthesis and related electrical tests of $Na_{2/3}Ni_{1/3}Mn_{2/3}O_2$ were carried out based on the previous report [40]. In Fig. S6a, the charge simulation of full cells shows appropriate voltage range of MWCNT-wrapped SiP_2 full cell obtained by subtracting the charge curve of NNMO from the discharge curve of the MWCNT-wrapped SiP_2 in their respective half cells. The MWCNT-wrapped SiP_2- NNMO charge curve full cell ranges from 0.8 V to 3.8 V, and the plateau of discharge curve is located between 2.0 to 3.0 V and 3.2–3.7 V, respectively. In Fig. S6b, the discharge curve of MWCNT-wrapped SiP_2//NNMO full cell was plotted in the same way, ranging from 3.2 to 1.0 V. The plateau of discharge curve is located between 1 to 2.2 V and 2.5–3.2 V, respectively. Therefore, the full cell cutoff voltage of discharge and charge should be set between 1.0 V and 4 V, respectively.

In Fig. 8a, a coin-typed full cell displays a specific capacity of 487 mA h g^{-1} at 0.05 A g^{-1} with good retention about 90.3% after 40 cycles (respect to 2nd cycle). The voltage profile of coin-typed full-cell at 1st, 10th, 20th and 30th cycle in Fig. 8b exhibits several potential plateaus during the discharge and charge cycles. In the charge process, potential plateaus locate between 2.0 and 3.7 V and in the discharge process, the voltage curve locates from 1.0 V to 3.7 V, both approximately correspond to the simulation result. As shown in Fig. 8c, the coin-typed full cell at high current density (2 A g^{-1}) exhibits high retention, i.e., 80%, with respect to the 2nd cycle after 100 cycles. In order to further facilitate MWCNT-wrapped SiP_2 applications, a 6 mA h pouch type full cell (Fig. 8d and e) was prepared and exhibits stable cycling performance up to 50 cycles. This cell can be used to light up more than 100 LEDs with 3 different colors (Fig. 8f).

2.1. Conclusion

In summary, we develop a facile way to wrap SiP_2 with MWCNT by using a ball milling porcess. MWCNT-wrapped SiP_2 shows high electrochemical performance with superior reversible capacity 1622 mA h g^{-1} in LIBs after 100 cycles, 925 mA h g^{-1} in SIBs after 200 cycles. In addition, MWCNT-wrapped SiP_2 composites also exhibit superior rate capabilities: 1522 mA h g^{-1} in LIBs at a current density of 4 A g^{-1} and 491 mA h g^{-1} in SIBs at a current density of 2 A g^{-1}, respectively, owing to five times higher electrical conductivity promoted by MWCNT. MWCNT not only plays a crucial role to provide robust network structure to mitigate mechanical strain and also effectively seizes the fragment of SiP_2 to surrounding electrical connections that prevents the capacity degradation. Pouch-type LIB (35 mA h) and SIB (6 mA h) were assembled to demonstrate practical uses. This study suggests that decoration of MWCNT can effectively enhance cycle performance and rate capability of SiP_2, making it a promising graphite alternative anodes for both LIBs and SIBs.

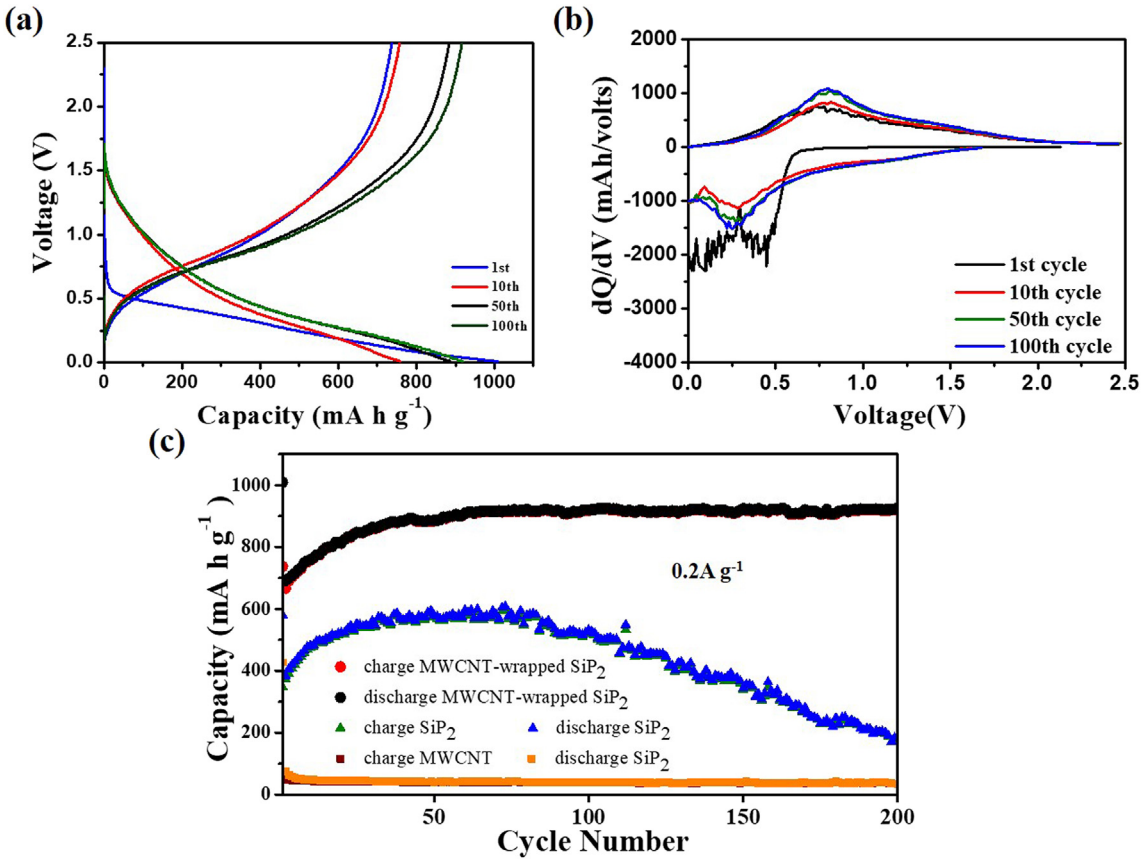

Fig. 6. Electrochemical performance of MWCNT-wrapped SiP_2 in SIBs (a) voltage profiles of MWCNT-wrapped SiP_2 at 0.1 A g^{-1} between 0.01 V and 2.5 V (b) differential capacity profiles of the first, 10th, 50th and 100th cycles of MWCNT-wrapped SiP_2. (c) cycle performance of MWCNT-wrapped SiP_2, SiP_2, and MWCNT at 0.1 A g^{-1} for 200 cycles.

Table 2
Comparison of the electrochemical performance of different SiP_2 electrodes for SIBs.

Active material	Capacity (5th cycle)	Capacity (200th cycle)	retention	Reference
MWCNT-wrapped SiP_2	715 mA h g^{-1}	925 mA h g^{-1}	129%	This work
SiP_2	430 mA h g^{-1}	185 mA h g^{-1}	43%	This work
SiP_2/C	~800 mA h g^{-1}	~400 mA h g^{-1} (15 cycle)	50%	[26]

3. Experimental section

3.1. Materials

Silicon (Si, powder, 325 mesh, 99% trace metals basis), poly (acrylic acid) (PAA, average MV ~3000000), ethanol (C_2H_5OH, 99.8%), sodium cubes (99.9%), sodium perchlorate ($NaClO_4$, 98%), manganese (II) carbonate ($MnCO_3$, 99.9%), sodium carbonate (Na_2CO_3, 99.5%), nickel (II) hydroxide ($Ni(OH)_2$), and ethylene carbonate (EC, 98%) were purchased from Sigma-Aldrich. Phosphorus (P, powder, 325mesh, 98.9%) was purchased from Alfa Aesar. MWCNT (90% O. D × L 10 nm × 1.5 μm) was purchased from Taiwan Carbon Nanotube Technology Corporation. Commercial $LiFePO_4$ was purchased from Vista Advance technology. Glass fiber filter was purchased from Toyo Roshi Kaisha, Ltd. Lithium hexafluorophosphate ($LiPF_6$), fluoroethylene carbonate (FEC, $C_3H_3FO_3$), diethyl carbonate (DEC, $C_5H_{10}O_3$), lithium metal foil, copper metal foil, Celgard membrane, and coin-type cell CR2032 were purchased from Shining Energy Co., Ltd.

3.2. Synthesis of MWCNT-wrapped SiP_2

Red P was transformed into black P by HEBM for 6 h, and then mixed with Si in 2:1 M ratio in a 12-ml grinding jar with 4 balls, where the ball-to-powder weight ratio was 160:1 with both the jar and the balls made in hardened stainless steel, and then SiP_2 powder was formed by 6-hrs HEBM under Ar atmosphere. SiP_2 powder and MWCNT were mixed in a 12-ml grinding jar with 5:3 wt ratio and 200:1 ball-to-powder weight ratio, followed by HEBM for 1 h with 200 RPM under Ar atmosphere, which led to the formation of MWCNT-wrapped SiP_2.

3.3. Characterization

MWCNT-wrapped SiP_2 was characterized by field emission scanning electron microscope (FESEM), Spherical Aberration Corrected Scanning Transmission Electron Microscope (Cs-corrected STEM), and X-ray diffraction (XRD). For SEM imaging, images were obtained by using a FESEM (HITACHI-SU8010) at an accelerating voltage of 10–15 kV with 8 mm working distance. The Cs-corrected STEM samples were prepared by dispersing the powder in the ethanol and drop-casting onto a carbon-coated copper grid, and the images were acquired by JEOL ARM200F at an accelerating voltage of 200 kV. XRD patterns were recorded by a Shimadzu XRD-6000 diffractometer equipped with CuK radiation.

3.4. Electrochemical characterization

MWCNT-wrapped SiP_2 and PAA were mixed in weight ratio of 80 wt %:20 wt% in ethanol to form homogeneous slurry, which was tape-casted on a copper foil and dried in an oven to prepare LIB or SIB electrodes. The electrodes were dried at 150° C for 1hr under argon gas

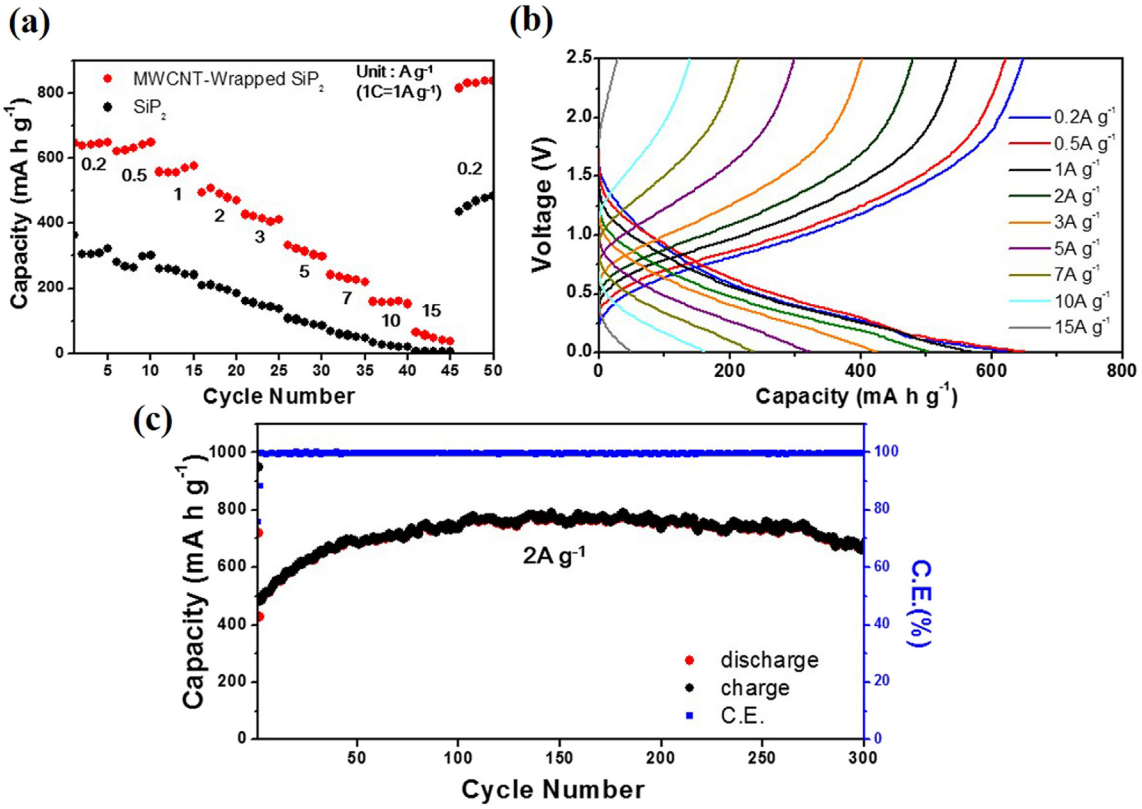

Fig. 7. (A) The rate performances of MWCNT-wrapped SiP_2 electrode at various current densities from 0.2 A g^{-1} to 15 A g^{-1} (b) the corresponding voltage profiles of (a) at various current densities from 0.2 A g^{-1} to 15 A g^{-1}(c) the cycling performance of MWCNT-wrapped SiP_2 at a current density 2 A g^{-1} over 300 cycles.

to remove residual water and then pressed by a rolling machine. The coin-type lithium-ion half cells (CR2032) contains MWCNT-wrapped SiP_2 composites electrode with a loading weight of ~1.5 mg cm^{-2}, a lithium metal foil, and a PP/PE/PP membrane wetted by electrolyte, were assembled in an argon-filled glovebox. The electrolyte was composed of 1 M $LiPF_6$ in a mixture of fluoroethylene carbonate/diethyl carbonate (FEC/DEC) (1:1 v/v). The electrochemical performance of the lithium half-cell was evaluated by using Maccor Series 4000 at the voltage range between 0.01 V and 2.0 V (vs. Li/Li^+).

As to the coin-type lithium ion full cell (CR2032), $LiFePO_4$ was used as the cathode with an A/C ratio of ~1.2, where the areal capacities of anode and cathode were 1.45 mA h cm^{-2} and 1.2 mA h cm^{-2}, respectively, and MWCNT-wrapped SiP_2 was used as the anode with loading weight of ~1.5 mg cm^{-2}. The rest of the components in the full-cell were identical with those in the half-cell. The electrochemical performance of the full cells was investigated by using Maccor Series 4000 at the voltage range between 2.0 V and 4.0 V. For the assembly of lithium ion pouch type batteries, the anode (MWCNT-wrapped SiP_2) and the cathode (commercial electrode $LiFePO_4$) were both tailored into rectangular shape with an area of 35 cm^2 (3.5 cm × 10 cm), then nickel tab and aluminum tab were connected to the anode and the cathode, respectively. The anode and the cathode separated by PP/PE/PP membrane were stacked evenly in a laminated Al film, which was then sealed, leaving one side open for later use. The semi-finished product was taken into a glovebox to be filled with electrolyte and sealed the unsealed side. The pouch type battery was also tested by using Maccor Series 4000 at the voltage range between 2.0 V and 4.0 V.

The coin-type sodium ion half cells containing a MWCNT-wrapped SiP_2 electrode with loading weight about 1.0 mg cm^{-2} (SiP_2 0.5 mg cm^{-2}), a sodium metal foil was pressed by roller from sodium cubes, and a glass fiber filter wetted by the electrolyte, were assembled in an argon-filled glovebox. The electrolyte was composed of 1 M $NaClO_4$ in a mixture of Propylene carbonate/fluoroethylene carbonate (EC:DEC:FEC) (4.5:4.5:1 v/v/v). The electrochemical performance of the sodium half-cell was tested by using Maccor Series 4000 at the voltage range between 0.01 V and 2.5 V (vs. Na/Na^+).

As to the coin-type sodium-ion full cells, NNMO was used as the cathode with an A/C ratio of ~1.0, where the areal capacities of anode and cathode were 0.35 mA h cm^{-2} and 0.348 mA h cm^{-2}, respectively, and MWCNT-wrapped SiP_2 was used as an anode with loading weight about 1.2 mg cm^{-2}. The synthesis of cathode material NNMO was based on the previous study [40]. The rest of components in full cells were identical with those in the half cells. The electrochemical performance of the sodium-ion full cells was examined at the voltage range between 1.0 V and 3.75 V. For sodium ion pouch type battery assembly, the anode (MWCNT-wrapped SiP_2) and the cathode (NNMO) were both cut into rectangular shape with an area of 30 cm^2 (3.3 cm × 9 cm), then nickel tab and aluminum tab were connected to the anode and the cathode, respectively. The anode and the cathode separated by PP/PE/PP membrane were stacked evenly in laminated Al film, which was then sealed, and left one side open for later use. The semi-finished product was taken into glovebox for filling electrolyte and sealing the unsealed side. The pouch type battery was tested by using Maccor Series 4000 at the voltage range between 1.0 V and 3.75 V.

CHARTS (Word Style "VB_Chart_Title"). Lists of structures may be called charts. Charts may have brief titles describing their contents. The title should follow the format "**Chart 1**. Chart Title". Charts may also have footnotes (use Word Style "FC_Chart_Footnote"). To insert the chart into the template, be sure it is already sized appropriately and paste it immediately after the chart title.

Acknowledgements

We acknowledge the financial support by the Ministry of Science and Technology through the grants of MOST 106-2221-E-007-081-MY3, 106-2628-E-007-005-MY3, and 103-2221-E-007-089-MY3, and

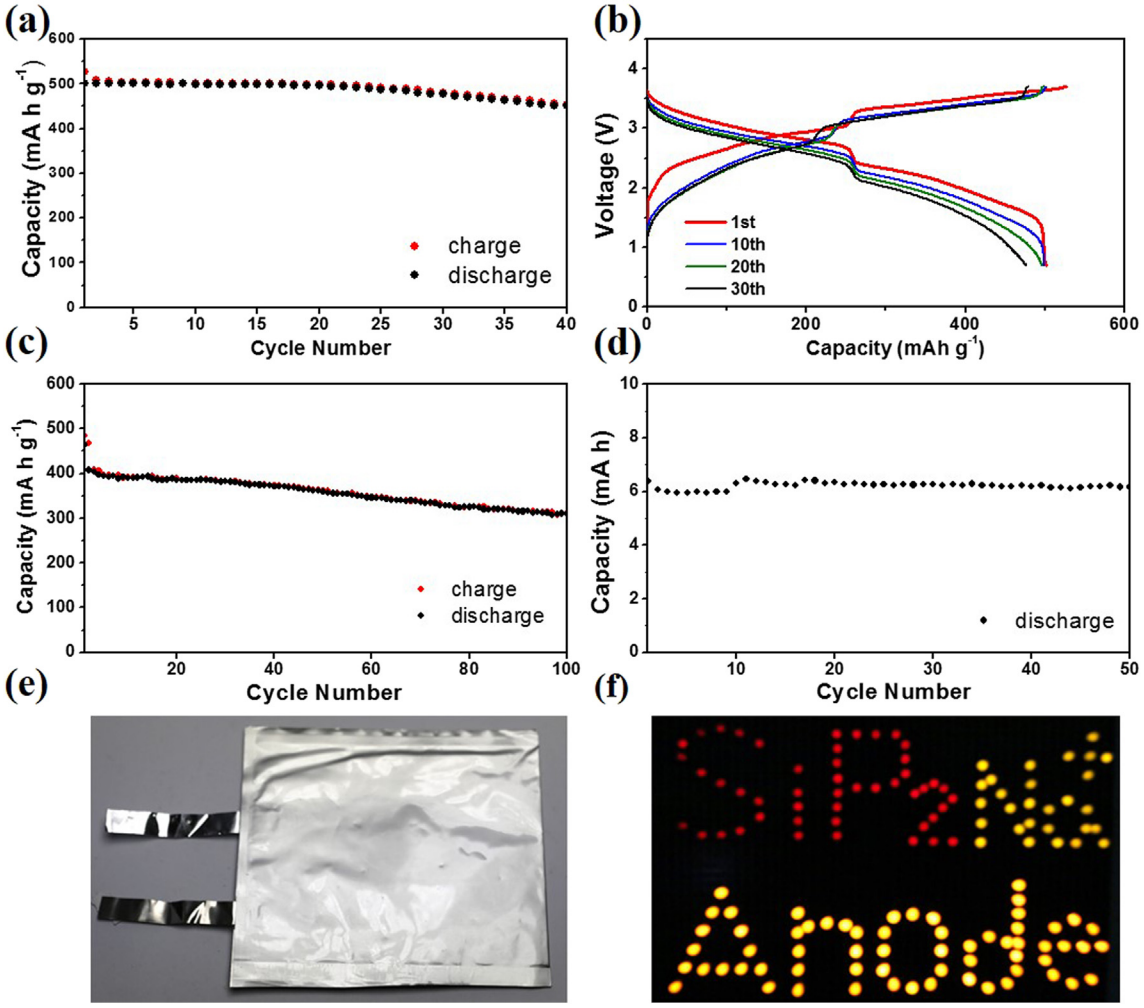

Fig. 8. Electrochemical characteristics of MWCNT-wrapped SiP_2-NNMO full cell. (a) cycling performance and (b) voltage profiles of a coin cell at a current density of 0.2 A g^{-1} between 1.0 V and 3.75 V. (c) cycling performance of coin cell at a current density of 2 A g^{-1} between 1.0 V and 3.75 V. (d) voltage profiles of 6 mA h pouch type cell at a current density of 0.2 A g^{-1} (e) the photograph of a 6 mA h pouch type battery. (f) the demonstration of the pouch-type battery lighting up over 100 LEDs with different colors. (For interpretation of the references to color in this figure legend, the reader is referred to the Web version of this article.)

MOST 106-2622-8-007-017.

Appendix A. Supplementary data

Supplementary data related to this article can be found at https://doi.org/10.1016/j.jpowsour.2018.07.003.

References

[1] L. Lu, X. Han, J. Li, J. Hua, M. Ouyang, J. Power Sources 226 (2013) 272–288.
[2] B. Scrosati, J. Garche, J. Power Sources 195 (2010) 2419–2430.
[3] P.R. Abel, A.M. Chockla, Y.-M. Lin, V.C. Holmberg, J.T. Harris, B.A. Korgel, A. Heller, C.B. Mullins, ACS Nano 7 (2013) 2249–2257.
[4] S. Goriparti, E. Miele, F. De Angelis, E. Di Fabrizio, R. Proietti Zaccaria, C. Capiglia, J. Power Sources 257 (2014) 421–443.
[5] J.-M. Tarascon, M. Armand, Nature 414 (2001) 359–367.
[6] N. Nitta, G. Yushin, Part. Part. Syst. Char. 31 (2014) 317–336.
[7] C.M. Hayner, X. Zhao, H.H. Kung, Annu. Rev. Chem. Biomol. Eng. 3 (2012) 445–471.
[8] W.-J. Zhang, J. Power Sources 196 (2011) 877–885.
[9] V. Etacheri, R. Marom, R. Elazari, G. Salitra, D. Aurbach, Energy Environ. Sci. 4 (2011) 3243–3262.
[10] Y.-L. Kim, H.-Y. Lee, S.-W. Jang, S.-H. Lim, S.-J. Lee, H.-K. Baik, Y.-S. Yoon, S.-M. Lee, Electrochim. Acta 48 (2003) 2593–2597.
[11] T. Kim, S. Park, S.M. Oh, Electrochem. Commun. 8 (2006) 1461–1467.
[12] H. Dong, R. Feng, X. Ai, Y. Cao, H. Yang, Electrochim. Acta 49 (2004) 5217–5222.
[13] F.F. Cao, J.W. Deng, S. Xin, H.X. Ji, O.G. Schmidt, L.J. Wan, Y.G. Guo, Adv. Mater. 23 (2011) 4415–4420.
[14] W.-S. Chang, C.-M. Park, J.-H. Kim, Y.-U. Kim, G. Jeong, H.-J. Sohn, Energy Environ. Sci. Technol. Humanit. 5 (2012) 6895–6899.
[15] J. Wolfenstine, J. Power Sources 124 (2003) 241–245.
[16] H. Kim, J. Choi, H.J. Sohn, T. Kang, J. Electrochem. Soc. 146 (1999) 4401–4405.
[17] L. Beaulieu, K. Hewitt, R. Turner, A. Bonakdarpour, A. Abdo, L. Christensen, K. Eberman, L. Krause, J. Dahn, J. Electrochem. Soc. 150 (2003) A149–A156.
[18] W.-C. Chang, K.-W. Tseng, H.-Y. Tuan, Nano Lett. 17 (2017) 1240–1247.
[19] L. Wang, X. He, J. Li, W. Sun, J. Gao, J. Guo, C. Jiang, Angew. Chem. Int. Ed. 51 (2012) 9034–9037.
[20] W.-J. Li, S.-L. Chou, J.-Z. Wang, H.-K. Liu, S.-X. Dou, Chem. Commun. 51 (2015) 3682–3685.
[21] W. Zhang, M. Dahbi, S. Amagasa, Y. Yamada, S. Komaba, Electrochem. Commun. 69 (2016) 11–14.
[22] W.-J. Li, Q.-R. Yang, S.-L. Chou, J.-Z. Wang, H.-K. Liu, J. Power Sources 294 (2015) 627–632.
[23] M.-P. Bichat, T. Politova, H. Pfeiffer, F. Tancret, L. Monconduit, J.-L. Pascal, T. Brousse, F. Favier, J. Power Sources 136 (2004) 80–87.
[24] G.-A. Li, C.-Y. Wang, W.-C. Chang, H.-Y. Tuan, ACS Nano 10 (2016) 8632–8644.
[25] H.-T. Kwon, C.K. Lee, K.-J. Jeon, C.-M. Park, ACS Nano 10 (2016) 5701–5709.
[26] D. Duveau, S.S. Israel, J. Fullenwarth, F. Cunin, L. Monconduit, J. Mater. Chem. 4 (2016) 3228–3232.
[27] W. Li, H. Li, Z. Lu, L. Gan, L. Ke, T. Zhai, H. Zhou, Energy Environ. Sci. 8 (2015) 3629–3636.
[28] C. Zhang, X. Wang, Q. Liang, X. Liu, Q. Weng, J. Liu, Y. Yang, Z. Dai, K. Ding, Y. Bando, J. Tang, D. Golberg, Nano Lett. 16 (2016) 2054–2060.
[29] Z. Yu, J. Song, M.L. Gordin, R. Yi, D. Tang, D. Wang, Adv. Sci. 2 (2015) 1400020.
[30] Y. Kim, Y. Park, A. Choi, N.-S. Choi, J. Kim, J. Lee, J.H. Ryu, S.M. Oh, K.T. Lee, Adv. Mater. 25 (2013) 3045–3049.
[31] J. Qian, D. Qiao, X. Ai, Y. Cao, H. Yang, Chem. Commun. 48 (2012) 8931–8933.
[32] A. Bai, L. Wang, J. Li, X. He, J. Wang, J. Wang, J. Power Sources 289 (2015) 100–104.
[33] J. Sun, G. Zheng, H.-W. Lee, N. Liu, H. Wang, H. Yao, W. Yang, Y. Cui, Nano Lett. 14

(2014) 4573–4580.
[34] D. Yuan, J. Cheng, G. Qu, X. Li, W. Ni, B. Wang, H. Liu, J. Power Sources 301 (2016) 131–137.
[35] W.-J. Li, S.-L. Chou, J.-Z. Wang, H.-K. Liu, S.-X. Dou, Nano Lett. 13 (2013) 5480–5484.
[36] Y. Zhao, H. Wang, H. Huang, Q. Xiao, Y. Xu, Z. Guo, H. Xie, J. Shao, Z. Sun, W. Han, X.F. Yu, P. Li, P.K. Chu, Angew. Chem. Int. Ed. 55 (2016) 5003–5007.
[37] A. Favron, E. Gaufrès, F. Fossard, A.-L. Phaneuf-L'Heureux, N.Y.W. Tang, P.L. Lévesque, A. Loiseau, R. Leonelli, S. Francoeur, R. Martel, Nat. Mater. 14 (2015) 826.
[38] A.R. Stegner, R.N. Pereira, K. Klein, R. Lechner, R. Dietmueller, M.S. Brandt, M. Stutzmann, H. Wiggers, Phys. Rev. Lett. 100 (2008) 026803.
[39] W.E. Spear, P.G. Le Comber, Solid State Commun. 17 (1975) 1193–1196.
[40] G. Liu, L. Wen, Y. Li, Y. Kou, Ionics 21 (2015) 1011–1016.